Received: 23 August 2021 | Revised: 4 August 2022 | Accepted: 9 August 2022

DOI: 10.33012/navi.553

ORIGINAL ARTICLE

Preliminary Analysis of BDS-3 Performance for ARAIM

Hengwei Zhang[1] | **Yiping Jiang**[1] | **Ling Yang**[2]

[1] Interdisciplinary Division of Aeronautical and Aviation Engineering, The Hong Kong Polytechnic University

[2] College of Surveying and Geo-Informatics, Tongji University

Correspondence
Yiping Jiang
Interdisciplinary Division of Aeronautical and Aviation Engineering
The Hong Kong Polytechnic University
Tel: 3400 8063
Email: yiping.jiang@polyu.edu.hk.

Abstract

To support the operation of advanced receiver autonomous integrity monitoring (ARAIM), an integrity support message indicating a minimum performance level of satellite constellation is required for aircraft navigation. With BDS-3 providing worldwide service since July 2020, it is desirable to undertake a detailed study on its signal-in-space range error characteristics and prior fault probabilities for ARAIM. The latest accuracy criteria released by the China Satellite Navigation Office in May 2021 is validated by the 27 MEO and IGSO satellites in orbit from July 2020 to June 2021, in which 10 single satellite faults were identified and analyzed in detail with no constellation fault found. Based on this one-year data, the probability of single satellite faults and constellation faults can be initially set as 8×10^{-5} and 1×10^{-3}, respectively, for BDS-3 in ARAIM.

1 | INTRODUCTION

With the modernization of GPS and other constellations becoming operational (e.g., GLONASS, Galileo, and BDS), advanced receiver autonomous integrity monitoring (ARAIM) has been developed by taking advantage of dual-frequency and multi-constellation measurements (Blanch et al., 2015). As an airborne application, ARAIM can support stringent services globally with vertical guidance (e.g., localizer precision vertical 200-feet decision height [LPV-200; Working Group C, 2015]). Since satellite signals may fail in the process of production, transmission, and reception, the developers of ARAIM developed an integrity support message (ISM) for bounding position error within the required integrity budget by the protection level (PL; Working Group C, 2016). ISMs consist of various integrity parameters including user range error (URE), user range accuracy (URA), probability of single satellite fault (P_{sat}), probability of constellation fault (P_{const}), and nominal bias (b_{nom}), which are statistical measures of the range error caused by the control and space segments.

URE refers to a 1σ bound of the nominal broadcast orbit and clock errors, while signal-in-space range error (SISRE) acts as the error, itself. URA is broadcast by constellation service providers—a satellite is considered to have a service failure if the global average SISRE is greater than 4.42-times the URA value (DoD, 2020). The probability of single satellite fault is defined as P_{sat}, while P_{const} is the probability that more than one satellite is faulty (Walter et al., 2019). Based on the ARAIM baseline algorithm (Working Group C, 2016), smaller P_{sat} and P_{const} values can result in more than necessary integrity risk allocated for the fault hypothesis with

possible non-conservative PLs generated. Conversely, overly large P_{sat} and P_{const} values may result in over-conservative PLs. Therefore, it is vital to determine appropriate estimates for P_{sat} and P_{const}.

There have been abundant works on the evaluation of SISRE from the perspective of constellation performance during service histories. GPS SISRE behaviors were characterized from 2008 to 2011 by Heng et al. (2011). Similar analyses were conducted for GLONASS (Heng et al., 2012), Galileo (Perea et al., 2016), and QZSS (Montenbruck et al., 2015, 2018). For BDS-2, the navigation message availability and SISRE performance were assessed from 2013 to 2018 for 14 satellites (Ouyang et al., 2019). The statistical characterization of SISRE was also preliminarily evaluated for BDS-3 (Lv et al., 2020; Xue et al., 2021). Furthermore, a comparison between BDS-2 and BDS-3 was conducted based on five years' data (Chen et al., 2021). However, the SISRE evaluation in the above works on BDS lack consideration of the independence between radial and clock errors. As for the fault probability analysis and validation of error bounds for ARAIM, GPS data from 2008 through 2015 was examined to bound the URA and P_{sat} values (Walter & Blanch, 2015). In addition, five single satellite faults were observed over seven years and presented in detail by Walter and Blanch (2015). Similar works were conducted for GLONASS (Walter et al., 2018) and Galileo (Perea et al., 2017). Nominal SISRE behaviors were captured, and fault probabilities were preliminarily suggested for all BDS-2 and a few BDS-3 satellites (Wang et al., 2021). However, it was assumed that the reference time of ephemeris would always match the transmission time of message in the SISRE evaluation scheme, which may underestimate fault probabilities. For BDS-3, related work is still ongoing along with the development of the constellation.

With BDS-3 providing full worldwide service, it is desirable to undertake a detailed study on its SISRE characteristics and fault events for BDS-3 to be used in ARAIM. The China Satellite Navigation Office (CSNO) released a statement in 2021 that full constellation service failures had not exceeded three times per year and the duration of failure had never exceeded six hours (CSNO, 2021). This statement is validated with one year's BDS-3 data in this paper for calculation of P_{sat} and P_{const} values in ARAIM.

The paper is organized as follows: First, the method for evaluating SISRE is described; second, SISRE behaviors during the first fully operational year are analyzed with a broadcast URA value; then, four SISRE accuracy standards and the broadcast URA value are validated based on observed historical data; and finally, each fault event is analyzed in detail with the resulting values for P_{sat} and P_{const}.

2 | SISRE COMPUTATION

SISRE is calculated by differencing the orbit and clock between broadcast and precise ephemerides, where the latter is regarded as the true value. To ensure the comparability of broadcast and precise orbit, time, and reference frame, antenna offset and clock correction are adjusted beforehand. For the time system, the precise ephemeris is referred to the GPS time system while the broadcast ephemeris is referred to the BDS time system. A BDS-GPS time offset of 14 s should be removed (Montenbruck et al., 2015). Although broadcast orbit uses the China Geodetic Coordinate System 2000 (CGCS2000) and precise orbit is referred to the International Terrestrial Reference Frame 2008 (ITRF2008), the realization of these two frames are commonly considered to agree at the few-centimeters' level (Wang et al., 2021). Since this difference is well below the uncertainty of broadcast

ephemerides, it can be disregarded in the following assessment. Antenna offset must be calibrated with the precise ephemeris aligned to the center of mass (CoM) and the broadcast ephemeris must also be referred to the satellite antenna phase center (APC; Heng et al., 2010). The value of the APC is obtained from the International GNSS Service (IGS) antenna phase center model (i.e., igs14.atx).

As for clock error, the precise and broadcast ephemerides cannot be compared directly. The precise clock offset, T_p, is based on the B1I and B3I signals while the broadcast clock offset, T_b, refers to the single-frequency B3I signal. Therefore, the time group delay (TGD) correction must be employed in the broadcast clock offset. The TGD_1 parameter in the broadcast ephemeris of BDS is used, in which TGD_1 is the TGD differential between the B1I and B3I signals (CSNO, 2018). The TGD correction for the broadcast clock is defined as:

$$TGD_{brdc} = \frac{f_1^2}{f_1^2 - f_3^2} TGD_1 \tag{1}$$

where f_1 and f_3 are the frequencies of the B1I and B3I signals, respectively.

There is a common bias, μ, of all satellites due to different timescales that varies from time to time (Montenbruck et al., 2015). The robust and iterative weighted-average method (Wu et al., 2017) is adopted here to estimate μ with a tolerance of potential clock outliers. Therefore, clock error as the difference between the broadcast and precise clock offsets is calculated by (Wang et al., 2021):

$$T = T_p - T_b + TGD_{brdc} - \mu \tag{2}$$

Different from GPS, BDS-3 adopts a two-way satellite time and frequency transfer (TWSTFT) method to calculate broadcast clock parameters (Zhou et al., 2016). Therefore, clock error is independent of orbit errors and the global average SISRE is calculated by (Wu et al., 2017):

$$URE_A = \sqrt{(\alpha \cdot R)^2 + T^2 + \beta^2 \cdot (A^2 + C^2)} \tag{3}$$

where R is the radial error, A is the along-track error, C is the cross-track error, T is the clock error, and α and β are weight factors as a function of the satellite altitude. With the mask angle set as 5°, the α and β values are set as 0.9823 and 0.1324, respectively, for medium Earth orbit (MEO) satellites, as well as 0.9924 and 0.0867, respectively, for inclined geosynchronous orbit (IGSO) satellites (Chen et al., 2021). To protect the most vulnerable users on Earth, the worst-case SISRE in the satellite's footprint is defined as (Heng et al., 2011):

$$URE_W = \max_{|\theta| \le \gamma} (R\cos\theta + T + \sqrt{A^2 + C^2}\sin\theta) \tag{4}$$

where θ is the satellite off-nadir angle and γ is the maximum off-nadir angle within one satellite's coverage (which is 18.13° for MEO and 13.64° for IGSO).

3 | DATA SOURCE

The BDS-3 broadcast and precise ephemerides collected from July 1, 2020, through June 30, 2021, were used for further analysis. The daily combined broadcast product was provided by the Multi-GNSS Experiment (MGEX) of the IGS (2022a) through collecting observation data from global tracking stations. However, the

broadcast product contained some erroneous records, e.g., incorrect PRN numbers and inconsistent reference time-of-clock, t_{oc}, values (Heng et al., 2010). Therefore, broadcast products from three different institutions, i.e., Crustal Dynamics Data Information System (CDDIS; CDDIS, 2021), Bundesamt für Kartographie und Geodäsie (BKG, 2021) and Test and Assessment Research Center (TARC) of CSNO (TARC of CSNO, 2021), were used to clean broadcast products (Wang et al., 2021). The detailed cleaning method is described as follows:

1. Least-significant bit (LSB) recovery is employed to convert virtually equal representations of the ephemeris and clock parameters into the same floating-point number in the computer's memory (Heng et al., 2010).
2. 17 robust parameters are used to find identical navigation messages for each satellite at each epoch (Heng, 2012). At least one transmission time of message (TTOM) parameter in the broadcast messages from the three institutions should satisfy the criteria $0 \le TTOM -$ reference time of ephemeris $(t_{oe}) \le 18$ s; otherwise, the data of this epoch is discarded (Walter et al., 2016). The remaining parameters in the navigation message (CSNO, 2018)—three clock correction parameters, space vehicle (SV) accuracy, satellite health indicator (SatH1), TGD_1, TGD_2, age of data clock (AODC), age of data ephemeris (AODE), PRN, BeiDou time (BDT) of week, and t_{oc}—are checked as follows: Except for AODC, AODE, and BDT of week, the other nine parameters have a direct influence on the SISRE evaluation, so these nine parameters must be consistent among the three institutions; otherwise, this epoch data is discarded. The AODC, AODE, and BDT of week should be consistent in at least two institutions, otherwise this epoch data is discarded.
3. The t_{oe} is used to determine which broadcast ephemeris should be selected for a given epoch by applying the criteria of $0 \le t_k - t_{oe} < 1\ h$ with t_k as the time at epoch k.
4. Normally, ephemeris parameters are updated at the start of every BDT hour and, therefore, t_{oe} would be an integer. A similar rule applies for t_{oc} (CSNO, 2018). The effective value of the PRN in these navigation messages is in the range of 1–63, and the valid healthy flag in the broadcast ephemeris is zero (CSNO, 2017). These rules are used to further filter out invalid broadcast data.

For the precise ephemeris, the Wuhan University (WUM) final product is used, and the Information and Analysis Centre (IAC) final product is considered as a backup if the WUM product were to go missing (IGS, 2022b). Until now, only WUM and IAC centers could provide the final precise product for BDS-3. Two criteria (Spofford & Remondi, 2022) are used to exclude invalid precise ephemerides:

- If the value of the orbit accuracy exponent is zero or 99
- If the orbit value is 0.000000 or the clock value is 999999.9999

With the exception of the three geostationary Earth orbit (GEO) satellites missing precise ephemeris values, all BDS-3 MEO and IGSO satellites are analyzed below. Figure 1 shows the availability of data for each satellite over the analysis period.

In Figure 1, PRNs 38, 39, and 40 are IGSO satellites, and the remaining 24 are MEO satellites. The blue lines indicate that a valid comparison between the broadcast and precise ephemerides was obtained. The red dots indicate that a satellite is missing the precise ephemeris on one of the days. The pink crosses mean that the broadcast ephemeris is set to be unhealthy, while the black squares indicate

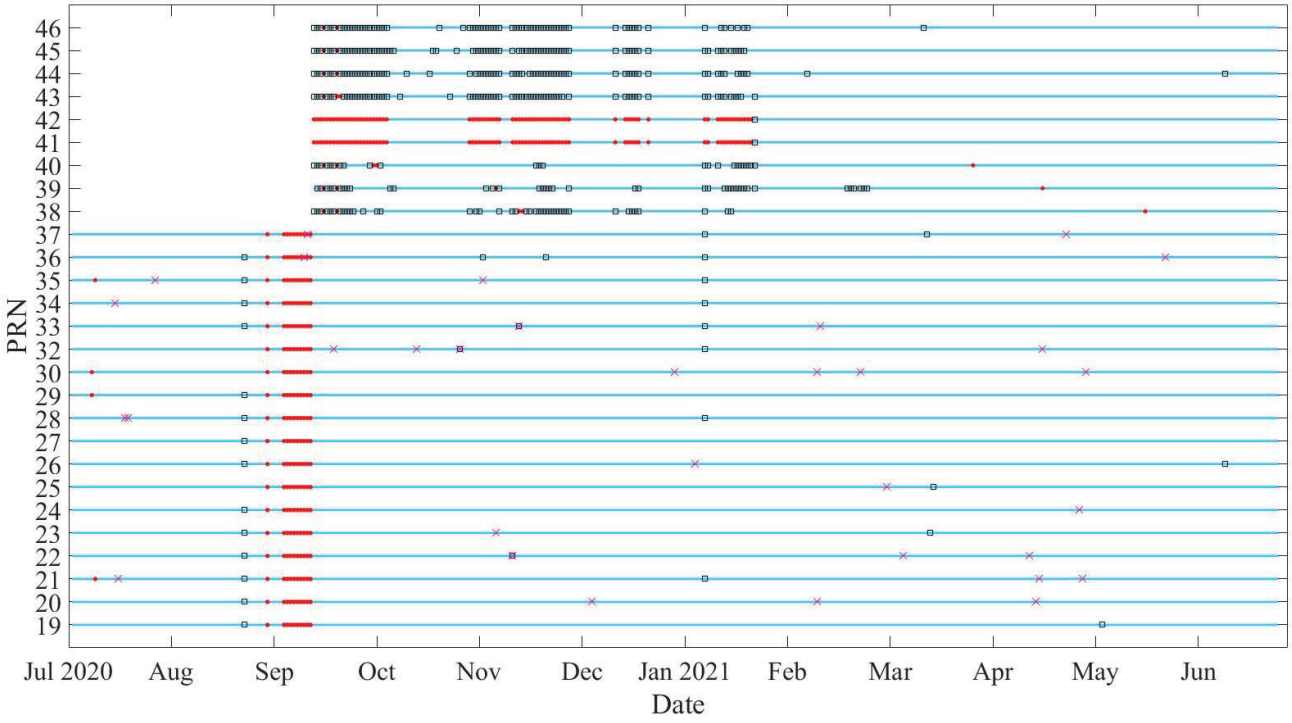

FIGURE 1 Availability of BDS-3 broadcast and precise data over the analysis period

the precise ephemeris is invalid at one epoch. In Figure 1, although two analysis centers were used to supplement each other, the final precise ephemerides still had some missing data, especially for PRNs 41 and 42. On one hand, the missing final precise data does not mean that there is likely to be a fault on that day (Wang et al., 2021). On the other hand, it is too optimistic to assume that none of these missing time periods contained any faulted behavior. Therefore, this work is regarded as a preliminary evaluation of P_{sat} and P_{const} in which the total valid satellite hours do not include any missing period(s).

4 | RESULTS AND DISCUSSION

The AODC and AODE are the extrapolated interval of clock correction parameters and ephemeris parameters, respectively. Therefore, smaller AODC and AODE values imply a higher accuracy of the broadcast parameters. Unlike GPS, BDS utilizes inter-satellite links (ISLs) for communication between satellites (Yang et al., 2017) to estimate broadcast ephemeris. Since the broadcast ephemeris is updated every hour, one hour is used to determine whether the broadcast ephemeris is up to date. Table 1 shows the percentage of AODC and AODE values larger than one hour for each satellite.

From Table 1, more than 99% of the AODC values and 98% of the AODE values were less than one hour, indicating that users could obtain the latest broadcast ephemeris most of the time. Compared to MEO satellites, IGSO satellites constrained to the Asia-Pacific region were observed by ground stations more frequently, but with the help of ISLs, the percentages of AODC and AODE values larger than one hour for MEO satellites showed no significant difference compared to the IGSO satellites shown in Table 1. For BDS-2, only 13.63% of the AODE values and 38.89% of the AODC values were less than one hour for MEO satellites (Wu et al., 2017), which

TABLE 1
Percentage of AODC and AODE Larger Than one Hour

PRN	AODC	AODE	PRN	AODC	AODE
19	0.39%	1.39%	34	0.24%	1.10%
20	0.37%	1.33%	35	0.40%	1.41%
21	0.82%	1.80%	36	0.47%	1.37%
22	0.77%	1.73%	37	0.69%	1.64%
23	0.34%	1.31%	38	0.36%	1.20%
24	0.37%	1.35%	39	0.33%	0.95%
25	0.34%	1.33%	40	0.27%	0.71%
26	0.56%	1.51%	41	0.29%	0.62%
27	0.58%	1.55%	42	0.28%	0.61%
28	0.39%	1.20%	43	0.40%	0.61%
29	0.66%	1.62%	44	0.55%	0.62%
30	0.67%	1.64%	45	0.54%	0.78%
32	0.34%	1.23%	46	0.46%	0.65%
33	0.50%	1.45%			

indicates a tremendous improvement observed in BDS-3. For PRNs 19 through 37, more than 50% of AODE values larger than one hour occurred during July 2020, which was the first month of BDS-3's official operation. After this period, less than 1% could be observed for the 20 satellites in question.

4.1 | SISRE Analysis

A satellite is considered to have a service failure if URE_A exceeds $4.42 \times URA$. To protect the most vulnerable user, a stricter criterion was used in the evaluation, i.e., $|URE_W| > 4.42 \times URA$ (Walter & Blanch, 2015). The URA is represented by a URA index (URAI) in the broadcast ephemeris with a relationship of $\text{URA} = 2^{\frac{\text{URAI}}{2}+1}$ (CSNO, 2018). It was observed that the URAI value was set to zero throughout the evaluation period. Accordingly, the upper bound of URA was 2.4 m, which was used to set the not-to-exceed (NTE) value to 10.61 m in order to detect failed satellites. After excluding these faults, orbit and clock errors were plotted for each satellite over the analysis period in Figure 2.

In Figure 2, the gap in the red-dashed rectangle is due to the missing precise ephemerides illustrated in Figure 1. For orbit errors, the radial error had the smallest value and the along-track error is similar to the cross-track error. To analyze error components in detail, Figure 3 further illustrates the mean and standard deviation for each satellite.

In Figure 3, the red dots indicate the mean and the blue bars show the length of twice the standard deviation. CASC and SECM represent two manufacturers (i.e., the China Aerospace Science and Technology Corporation and Shanghai Engineering Center for Microsatellites, respectively; TARC of CSNO, 2022). Rb and HM are Rubidium and Hydrogen atomic clocks, respectively. For orbit errors, the means were very close to zero in three directions for all satellites. As pointed out in Montenbruck et al. (2015), the APC offset used by IGS analysis centers is different from the value used by the GPS control center. This inconsistency primarily affects radial error. However, it is shown here that the means of the radial components

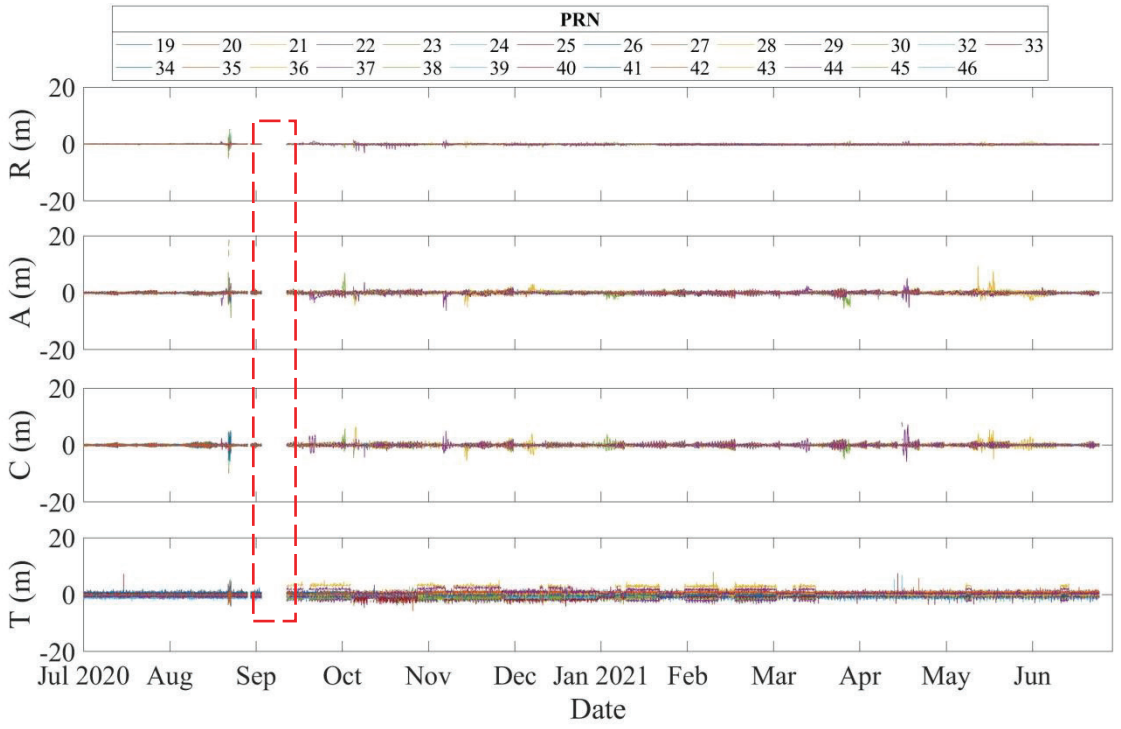

FIGURE 2 Time series of orbit and clock errors for each satellite: From top to bottom are (R) radial, (A) along-track, (C) cross-track, and (T) clock errors.

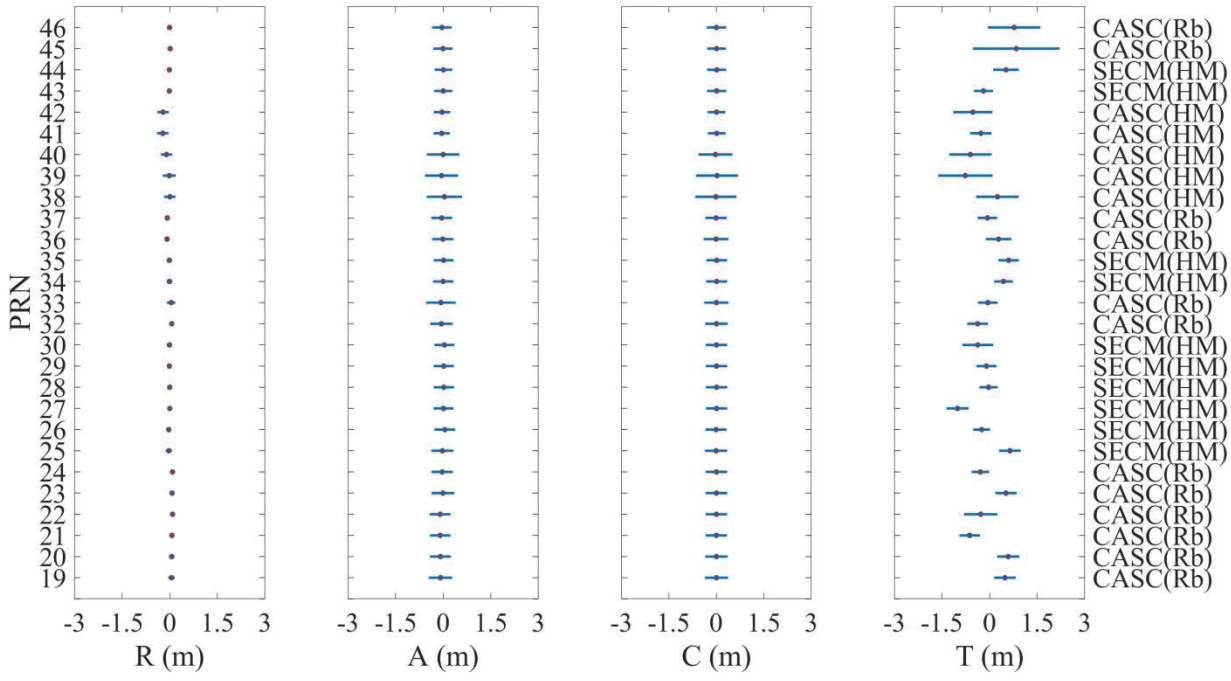

FIGURE 3 The mean and standard deviation of orbit and clock errors

were very close to zero for all satellites. Therefore, it can be concluded that the APC offsets used by IGS analysis centers and the BDS control center were the same. The standard deviations of radial, along-track, and cross-track errors were 0.10 m, 0.35 m, and 0.36 m, respectively, averaging all satellites together.

TABLE 2
Four SISRE Accuracy Standards

Symbol	A	B	C	D
Accuracy Standard	SISRE (95%, statistical value of all satellites)	SISRE (95%, statistical value of any single satellite)	SISRE (99.94%, average value over all the points on the global of any single satellite)	SISRE (99.79%, the worst case globally of any single satellite)
Threshold (m)	≤ 2	≤ 4.6	≤ 15	≤ 15
Numerical Results (m)	1.0728	1.5840	5.9477	4.0592

Compared with the results of BDS-2 (Wu et al., 2017), the standard deviation of along-track errors could reach 6 m to 8 m for a few satellites, while radial and cross-track errors achieved a standard deviation of roughly 1–2 m for all satellites, respectively. For the clock error, the bias was larger than orbit errors and obvious differences exist across the different satellites. Among the 27 satellites, the clock bias of PRN 27 was the largest with –1.01 m. Categorized by clock type, the averaged bias of the Hydrogen clock satellites was 0.44 m, which is similar to the Rubidium clock satellites' bias of 0.43 m.

It's also important to consider that satellite design varies by manufacturer. The averaged biases of satellites by manufacturers SECM and CASC were 0.41 m and 0.45 m, respectively. Therefore, different manufacturers and clock types had no obvious influence on bias. The six largest standard deviations of clock errors (i.e., 1.36 m, 0.83 m, 0.82 m, 0.67 m, 0.66 m, and 0.62 m) came from PRNs 45, 39, 46, 38, 40, and 42, respectively, which were all manufactured by CASC. In addition, the averaged standard deviation of all CASC satellites was 0.52 m compared to the 0.32 m for SECM satellites with better stability. In terms of the clock error for BDS-2 (Wu et al., 2017), a 1-m standard deviation was observed for most satellites, the largest reaching 2 m. It is obvious that the BDS-3 performance improves greatly using ISLs.

The four accuracy criteria issued by CSNO (2021) are illustrated in Table 2. The standards A and B are calculated for a period of seven days, and for standards C and D, a one-year period is required.

The four statistical results were calculated by the accuracy standards defined in Table 2 with standards A and B calculated from data from March 7, 2021, through March 13, 2021, and the one-year evaluation data was used to calculate standards C and D. Comparing the numerical results with the thresholds in Table 2, it is clear that the four SISRE criteria are satisfied.

4.2 | URA Validation

URA captures nominal SISRE behaviors, and if $|URE_W|/\text{URA}$ exceeds a value of 4.42, it is regarded as a fault. Figure 4 shows one minus the cumulative distribution function (CDF) of $|URE_W|/\text{URA}$ for each satellite and satellites grouped by type.

In Figure 4, the rightmost heavy red line represents a normal distribution with a unit variance and mean at 0.75 m, which is used as the b_{nom} value for GPS (Walter et al., 2018). Whether or not satellites fall above or below the red line is largely dependent on the total amount of data (Walter et al., 2015), which means that satellites with shorter histories are more likely to fall above in Figure 4.

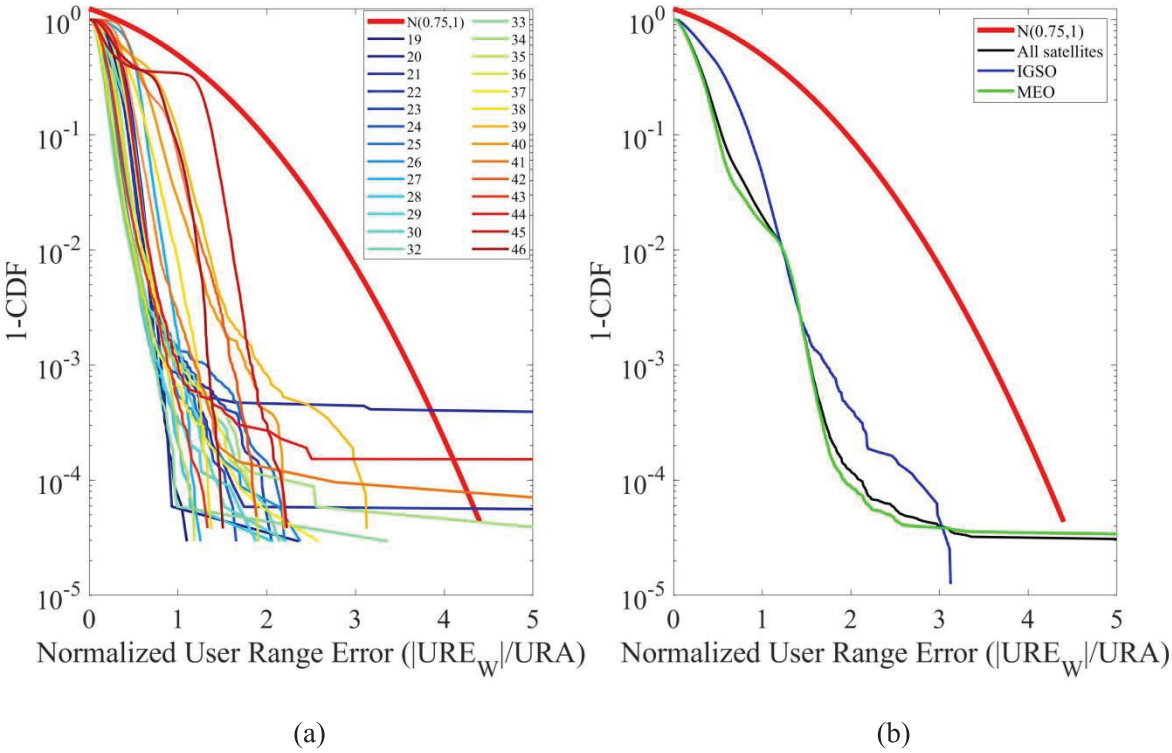

FIGURE 4 1 – CDF of normalized $|URE_W|$/URA: (a) represents individual satellites and (b) represents satellites grouped by type

In Figure 4(a), due to single satellite faults that are analyzed later in Section 4.3, five satellites (i.e., PRNs 21, 22, 34, 41, and 44) fall above the red line. Although eight satellites are affected by single faults, the other three faults are sufficiently short and small, having little impact on the CDF. In Figure 4(b), the black line is closer to the green line because only three IGSO satellites are involved in the total data compared with 24 MEO satellites. For the two types of satellites (i.e., MEO and IGSO), the nominal orbit and clock errors can be conservatively described by the broadcast URA. As mentioned in Section 3, there are some missing data during the evaluation period. Therefore, the validation of URA is preliminary.

4.3 | Fault Analysis

During the analysis period, the upper bound of the URA was 2.4 m, and the threshold was 10.61 m (indicated as the horizontal red line in the following figures of $|URE_W|$). To further validate the results, the fault condition was double-checked by precise products from two analysis centers—one from Shanghai Observatory (SHAO) and one from GeoForschungsZentrum Potsdam (GFZ; IGS, 2022b). In total, 10 single satellite faults and zero constellation faults were identified over the first fully operational year, as summarized in Table 3.

Each fault event was analyzed in detail by combining the precise orbit products of 15-min intervals with precise clock products of 30-s intervals from WUM. Through the Lagrange method, precise orbit was interpolated to have 30-s intervals and aligned with the clock product. Figure 5 shows the PRN-20 fault event on April 18, 2021.

TABLE 3
Information of 10 Single Satellite Faults

PRN	IGS-SVN	Clock Type	Date	GPST (hh:mm:ss)
20	C202	Rubidium	April 18, 2021	07:39:00–07:48:18
21	C206	Rubidium	July 15, 2020	11:18:30–11:36:18
			April 30, 2021	16:44:00–18:59:30
			May 2, 2021	10:24:30–10:59:30
				14:32:30–14:59:30
22	C207	Rubidium	November 11, 2020	06:25:00–06:48:00
33	C215	Rubidium	February 12, 2021	06:35:00–06:48:18
34	C216	Hydrogen	July 14, 2020	09:23:30–09:48:18
37	C219	Rubidium	April 27, 2021	03:43:00–03:48:18
41	C227	Hydrogen	January 2, 2021	01:23:00–01:48:00
44	C225	Hydrogen	January 10, 2021	22:00:00–22:59:30

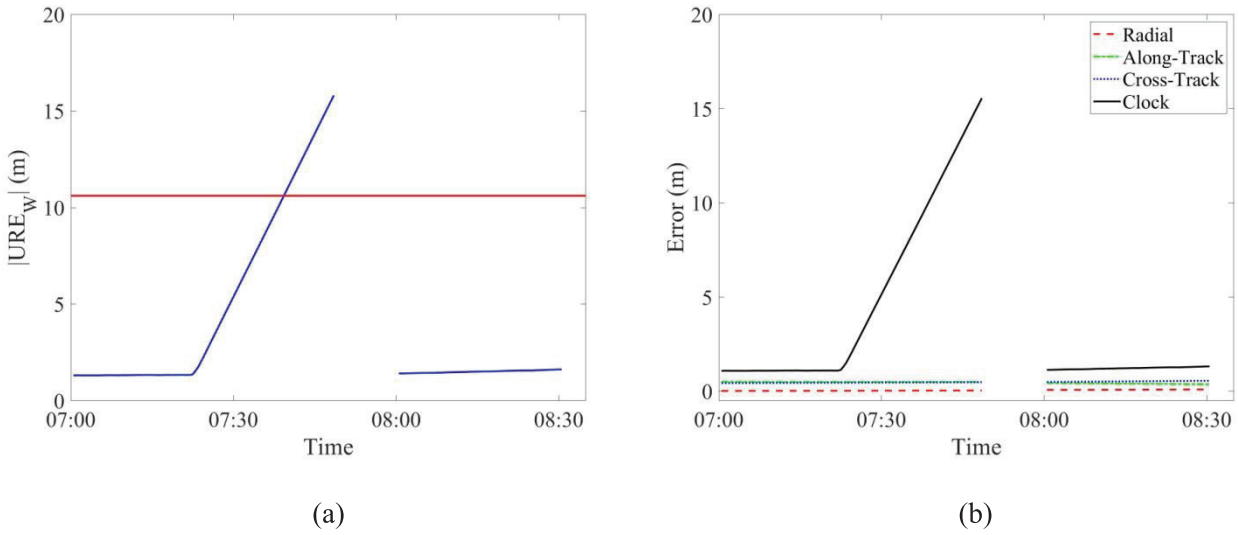

FIGURE 5 Fault event of PRN 20 on April 18, 2021: (a) represents $|URE_W|$ and (b) represents orbit and clock errors

From Figure 5(b), it is obvious that this fault was a clock ramp, which started at 07:39:00 and lasted 9.3 minutes. The clock error began to increase gradually at 07:22 and was larger than the threshold at 07:39. At 07:48:18, users received a broadcast ephemeris notifying them that the satellite was unhealthy. This was the reason why $|URE_W|$ values were missing between 07:48:18 and 8:00. The clock error resumed to normal by 08:00 due to a new broadcast ephemeris update.

For PRN 21, a fault event lasting 135.5 minutes occurred on April 30, 2021, as shown in Figure 6. From Figure 6(b) and 6(c), this fault was due to a sudden clock jump, which began at 16:44 when the AODC was one hour. From Figure 6(d), the AODC was one and two hours at 17:00 and 18:00, respectively, when two broadcast ephemerides updated. These two new broadcast ephemerides caused two discontinuities in the clock error in Figure 6(c) without correcting the clock drift. At 19:00, an updated broadcast ephemeris corrected the clock error to be around 0 m,

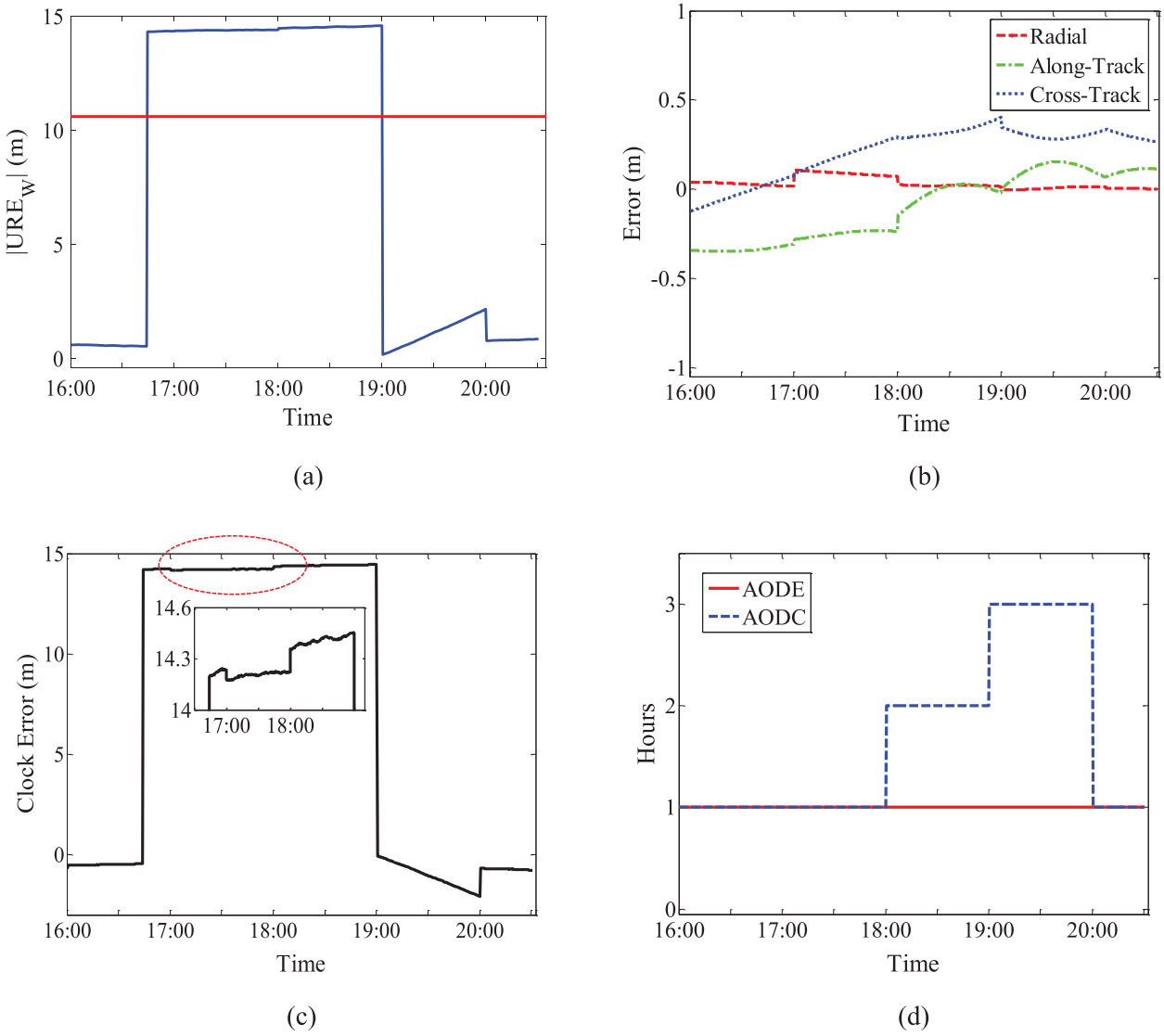

FIGURE 6 Fault event of PRN 21 on April 30, 2021: (a) represents $|URE_W|$, (b) represents orbit error, (c) represents clock error, and (d) represents AODE and AODC.

effectively ending the fault event. However, the AODC was three hours, resulting in an increased trend of the clock error between 19:00 and 20:00 without causing a fault event again. At 20:00, the broadcast ephemeris updated with the AODC at one hour and the clock error became normal.

In Figure 7, it became obvious that this fault was due to a clock jump. The clock jump started at 10:24:30 and reached its maximum value of 83 m at 10:57:30 until a new broadcast ephemeris updated at 11:00 with SatH1=1, indicating that the satellite was unhealthy. Fortunately, the clock error resumed to normal at 12:00 with a new broadcast ephemeris set with SatH1=0. However, the clock error became larger than the threshold again at 14:32:30 when the satellite was flagged unhealthy once again at 15:00 by a new broadcast ephemeris. Two hours later, a new broadcast ephemeris with SatH1=0 was received at 17:00, indicating the satellite was healthy again and the clock error became normal.

Figure 8 shows the fault event affecting PRN 22 on November 11, 2020. Different from the clock ramp in Figure 5(b), this fault event was caused by a sudden clock jump. From Figure 8(a), this fault started at 06:25 and the maximum value was

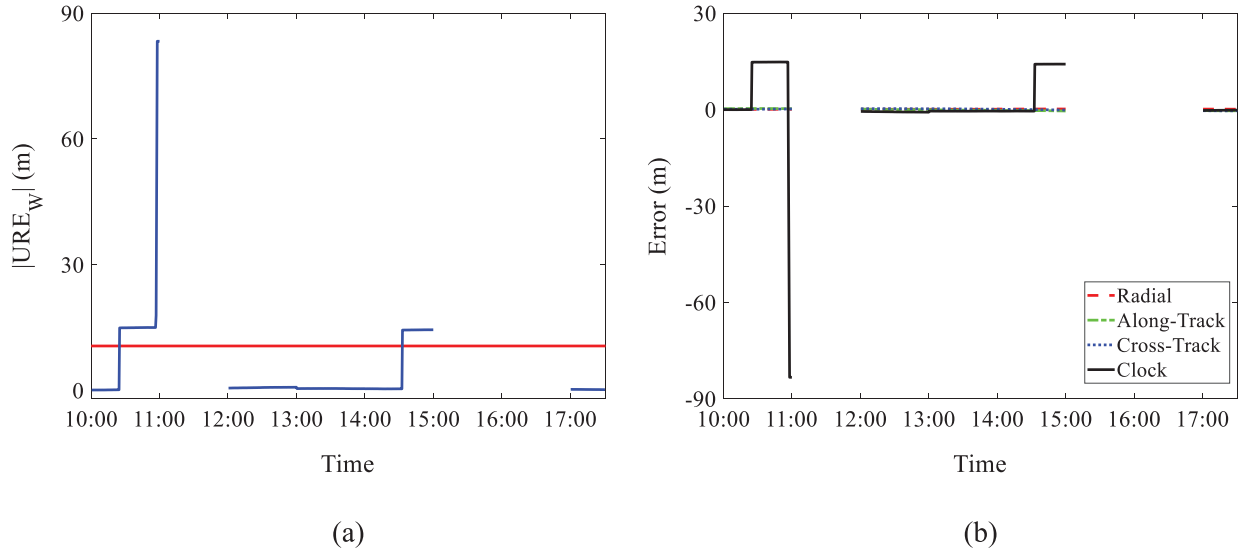

FIGURE 7 Fault event of PRN 21 on May 2, 2021: (a) represents $|URE_W|$ and (b) represents orbit and clock errors

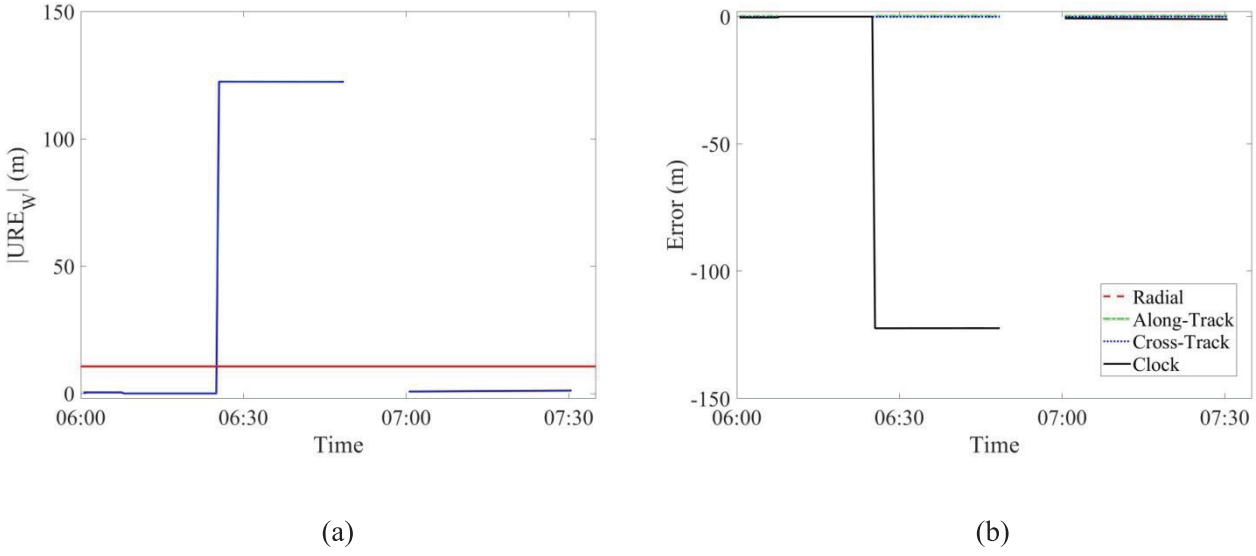

FIGURE 8 Fault event of PRN 22 on November 11, 2020: (a) represents $|URE_W|$ and (b) represents orbit and clock errors

around 122 m. At 06:48, a broadcast ephemeris was received and notified that the satellite was unhealthy. The clock error resumed to normal at 07:00 due to a new broadcast ephemeris update.

For PRN 44, a fault event on January 10, 2021, is shown in Figure 9. This was caused by a fault related to orbit errors lasting 59.5 min. From Figure 9(b) and 9(d), we can see that the AODE became two hours at 22:00 and orbit errors started to increase gradually at the same time. More than 120 km of along-track and cross-track errors were observed at 23:00. Although the AODC also reached two hours at 22:00, a discontinuity was observed in the clock error in Figure 9(c) without large error. The broadcast ephemeris updated and the AODE became one hour when the orbit errors were reset at 23:00. Since the other five events of PRNs

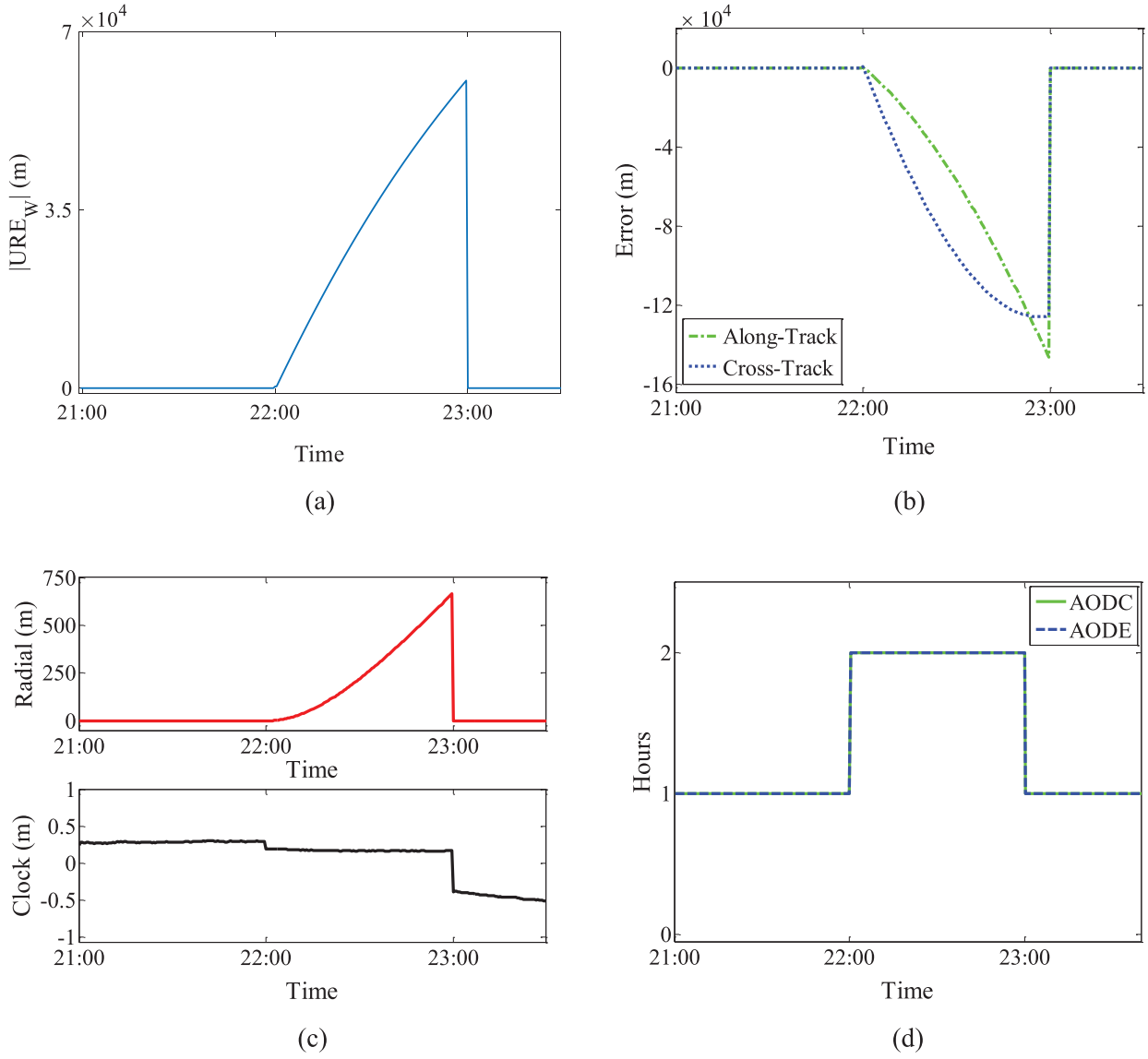

FIGURE 9 Fault event of PRN 44 on January 10, 2021: (a) represents $|URE_W|$, (b) represents along-track and cross-track errors, (c) represents radial and clock errors, and (d) represents AODE and AODC

21 (July 15, 2020), 33, 34, 37, and 41 caused by the clock ramp are similar to the PRN-20 fault shown in Figure 5, detailed descriptions are saved here.

Except for the two fault events from PRNs 21 (April 30, 2021) and 44, all the other events set satellites as unhealthy sometime after the onset of the fault. Among the 10 single satellite faults, nine faults were caused by the clock error, which indicates that the onboard clock had a great influence on the performance of BDS-3. In addition, in these nine fault events, PRN 20, 21, 22, 33, and 37 satellites equipped with Rubidium clocks suffered seven faults for a total of 266.2 min, while PRN 34 and PRN 41 satellites with Hydrogen clocks had two faults for a total of 49.8 min. During the evaluation period, the operational time for 12 Rubidium and 15 Hydrogen satellites was 5,837,865 min and 6,622,695 min, respectively. The relative operating percentage for each clock type did not differ much. Therefore, better performance can be expected for BDS-3 when new satellites equipped with Hydrogen clocks are launched.

The probability of a single satellite fault (P_{sat}) and constellation fault (P_{const}) were calculated by (Walter et al., 2019):

$$\begin{aligned} P_{sat} &= MTTN_{sat} \times R_{sat} \\ P_{const} &= MTTN_{const} \times R_{const} \end{aligned} \tag{5}$$

where $MTTN_{sat}$ and $MTTN_{const}$ represent the averaged fault duration for single satellite and constellation faults, respectively. R_{sat} and R_{const} are the satellite fault rate per hour for single and constellation faults, respectively. Furthermore, the satellite fault rate R is calculated by (Walter et al., 2019):

$$R = \frac{N_F + \frac{1}{2}}{T_t} \tag{6}$$

where N_F is the number of fault events within a total time interval, T_t. This equation ensures that the evaluation result is consistent across satellite fault rate and mean time between faults (Walter et al., 2019; Wang et al., 2021). PRN 21 had three faults over the course of one year, indicating that it violates the assumption that a fault occurring in one time interval does not affect the probability of it occurring in other time intervals (Walter et al., 2019). Therefore, the fault rate formula is not truly applicable to PRN 21 and the estimated fault rates in the following analysis are only preliminary.

Less than three full constellation service failures per year with a failure duration less than six hours is stated from the CSNO statement (2021). Although this statement is not a commitment, it can be regarded as a standard to be compared with the observed value. Firstly, standard values are calculated by Equation (6) based on the above statement. The upper bounds of R and $MTTN$ are calculated as follows: $R_{sat\_upper} = \frac{3+\frac{1}{2}}{30\times365\times24} = 1.33\times10^{-5}$/hour, $R_{const\_upper} = \frac{1+\frac{1}{2}}{365\times24} = 1.71\times10^{-4}$/hour, and $MTTN_{sat\_upper} = MTTN_{const\_upper} = 6$ hours. The product of R and $MTTN$ implies an upper bound for the probabilities $P_{sat\_upper} = R_{sat\_upper} \times MTTN_{sat\_upper} = 8\times10^{-5}$ and $P_{const\_upper} = 1\times10^{-3}$.

Then, historically observed values were obtained based on one year of observation. The total cumulative duration of the 10 single satellite faults was 375.5 min among the 12,460,560 valid minutes. Therefore, $R_{sat} = \frac{10+\frac{1}{2}}{12460560\div60} = 5.06\times10^{-5}$/hour and $MTTN_{sat}$ is 37.55 min. Although the R_{sat} is larger than R_{sat_upper}, the P_{sat} obtained as 3.16×10^{-5} is smaller than P_{sat_upper}. Since no constellation fault was been observed for BDS-3 within the observed year, it would be prudent to set the P_{const} value to correspond to at least one more fault than what has actually been observed (Walter et al., 2019), especially for a new constellation. Therefore, the P_{sat} and P_{const} values by CSNO (2021), i.e., 8×10^{-5} and 1×10^{-3}, are safe to be used for ARAIM. Since BDS-3 has announced its official operation at the end of July 2020, and also considering the missing data during the analysis period, this evaluated work can only provide a preliminary overview of constellation performance, thus, the estimated P_{sat} and P_{const} values are not definitive.

5 | CONCLUSION

The SISRE of all BDS-3 MEO and IGSO satellites from July 1, 2020, to June 30, 2021, were evaluated and characterized. For orbit errors, the means were very close to zero in all three directions for all satellites. The standard deviations of radial, along-track, and cross-track errors were 0.10 m, 0.35 m, and 0.36 m, respectively,

by averaging all satellites together. For the clock error, the deviation from zero was larger than the orbit errors and obvious differences exist between different sat-ellites. It was demonstrated that the BDS-3 performance met the requirement of accuracy criteria over the analysis period.

For the two types of satellite orbits (i.e., MEO and IGSO), the nominal orbit and clock errors could be conservatively described by the broadcast URA. During the first fully operational year, 10 single satellite faults were identified, and no constel-lation fault occurred. Among the 10 single satellite faults, nine of the faults were caused by the clock error, which indicates that the onboard clock has great influ-
ence on the performance of BDS-3. The P_{sat} and P_{const} values can be initially set to 8×10^{-5} and 1×10^{-3}, respectively, in ARAIM ISMs. Since BDS-3 announced its official operation at the end of July 2020 and there was some missing data during the analysis period, this evaluation can only provide a preliminary overview of constellation performance. The estimated P_{sat} and P_{const} values are, thus, not definitive.

ACKNOWLEDGMENTS

The work in this paper is funded by NSFC (Grant no. 42004029) and RGC (Grant no.25202520). This support is gratefully acknowledged.

REFERENCES

Blanch, J., Walker, T., Enge, P., Lee, Y., Pervan, B., Rippl, M., Spletter, A., & Kropp, V. (2015). Baseline advanced RAIM user algorithm and possible improvements. *IEEE Transactions on Aerospace and Electronic Systems*, *51*(1), 713–732. https://doi.org/10.1109/TAES.2014.130739

Bundesamt für Kartographie und Geodäsie (BKG). (2021). *Navigational GNSS data and products*. https://igs.bkg.bund.de/root_ftp/IGS/BRDC

(CDDIS). (2021). *International GNSS Service: daily navigation data*. https://cddis.nasa.gov/archive/gnss/data/daily

Chen, G., Zhou, R., Hu, Z., Lv, Y., Wei, N., & Zhao, Q. (2021). Statistical characterization of the signal-in-space errors of the BDS: a comparison between BDS-2 and BDS-3. *GPS Solutions*, *25*(3). https://doi.org/10.1007/s10291-021-01150-x

China Satellite Navigation Office (CSNO). (2017). *BeiDou Navigation Satellite System signal in space interface control document: open service signal B1C* (Version 1.0). http://www.beidou.gov.cn/xt/gfxz/201712/P020171226741342013031.pdf

China Satellite Navigation Office (CSNO). (2018). *BeiDou Navigation Satellite System signal in space interface control document: open service signal B3I* (Version 1.0). http://www.beidou.gov.cn/xt/gfxz/201802/P020180209623601401189.pdf

China Satellite Navigation Office (CSNO). (2021). *BeiDou Navigation Satellite System open service performance standard* (Version 3.0). http://www.beidou.gov.cn/xt/gfxz/202105/P020210526216231136238.pdf

EU-U.S. Working Group C-ARAIM Technical Subgroup (Working Group C). (2015). *Milestone 2 report.* https://www.gps.gov/policy/cooperation/europe/2015/working-group-c/ARAIM-milestone-2-report.pdf

EU-U.S. Working Group C-ARAIM Technical Subgroup (Working Group C). (2016). Milestone 3 report. https://www.gps.gov/policy/cooperation/europe/2016/working-group-c/ARAIM-milestone-3-report.pdf

Heng, L., Gao, G. X., Walter, T., & Enge, P. (2010). GPS ephemeris error screening and results for 2006–2009. *Proc. of the 2010 International Technical Meeting of the Institute of Navigation*, San Diego, CA, 1014–1022. https://www.ion.org/publications/abstract.cfm?articleID=8881

Heng, L., Gao, G. X., Walter, T., & Enge, P. (2011). Statistical characterization of GPS signal-in-space errors. *Proc. of the 2011 International Technical Meeting of the Institute of Navigation*, San Diego, CA, 312–319. https://www.ion.org/publications/abstract.cfm?articleID=9472

Heng, L., Gao, G. X., Walter, T., & Enge, P. (2012). Statistical characterization of GLONASS broadcast clock errors and signal-in-space errors. *Proc. of the 2012 International Technical Meeting of the Institute of Navigation*, Newport Beach, CA, 1697–1707. https://www.ion.org/publications/abstract.cfm?articleID=10044

Heng, L. (2012). *Safe satellite navigation with multiple constellations: global monitoring of GPS and GLONASS signal-in-space anomalies*. [Doctoral dissertation, Stanford University]. https://web.stanford.edu/group/scpnt/gpslab/pubs/theses/LHengThesisFinalSignedSecured.pdf

International GNSS Service (IGS). (2022a). *MGEX pilot project.* https://igs.org/mgex

International GNSS Service (IGS). (2022b). *MGEX data & products.* https://igs.org/mgex/data-products/#orbit_clock

Lv, Y., Geng, T., Zhao, Q., Xie, X., & Zhou, R. (2020). Initial assessment of BDS-3 preliminary system signal-in-space range error. *GPS Solutions*, *24*(1). https://doi.org/10.1007/s10291-019-0928-x

Montenbruck, O., Steigenberger, P., & Hauschild, A. (2015). Broadcast versus precise ephemerides: a multi-GNSS perspective. *GPS Solutions*, *19*(2), 321–333. https://doi.org/10.1007/s10291-014-0390-8

Montenbruck, O., Steigenberger, P., & Hauschild, A. (2018). Multi-GNSS signal-in-space range error assessment—methodology and results. *Advances in Space Research*, *61*(12), 3020–3038. https://doi.org/10.1016/j.asr.2018.03.041

Ouyang, C., Shi, J., Shen, Y., & Li, L. (2019). Six-Year BDS-2 broadcast navigation message analysis from 2013 to 2018: availability, anomaly, and SIS UREs assessment. *Sensors*, *19*(12), 2767. https://doi.org/10.3390/s19122767

Perea, S., Meurer, M., Martini, I., Rippl, M., Joerger, M., & Pervan, B. (2016). Nominal range error analysis to support ARAIM. *Proc. of the 29th International Technical Meeting of the Satellite Division of the Institute of Navigation (ION GNSS+ 2016)*, Portland, OR, 1726–1735. https://doi.org/10.33012/2016.14861

Perea, S., Meurer, M., Rippl, M., Belabbas, B., & Joerger, M. (2017). URA/SISA analysis for GPS and Galileo to support ARAIM. *NAVIGATION*, *64*(2), 237–254. https://doi.org/10.1002/navi.199

Spofford, P. R., & Remondi, B. W. (2022). *The national geodetic survey standard GPS format SP3.* https://files.igs.org/pub/data/format/sp3_docu.txt

Test and Assessment Research Center (TARC) of China Satellite Navigation Office (CSNO). (2021). *Data services*. http://www.csno-tarc.cn/en/datacenter/ephemeris

Test and Assessment Research Center (TARC) of China Satellite Navigation Office (CSNO). (2022). *Constellation status* [Data set]. http://www.csno-tarc.cn/en/system/constellation

US Department of Defense (DoD). (2020). *Global Positioning System standard positioning service performance standard* (5th edition). https://www.gps.gov/technical/ps/2020-SPS-performance-standard.pdf

Walter, T. & Blanch, J. (2015). KEYNOTE–Characterization of GNSS clock and ephemeris errors to support ARAIM. *Proc. of the ION 2015 Pacific PNT Meeting,* Honolulu, HI, 920–931. https://www.ion.org/publications/abstract.cfm?articleID=12769

Walter, T., Gunning, K., & Blanch, J. (2016). Improved ephemeris monitoring for GNSS. *Proc. of the 2016 International Technical Meeting of the Institute of Navigation*, Monterey, CA, 600–608. https://doi.org/10.33012/2016.13414

Walter, T., Gunning, K., Phelts, R. E., & Blanch, J. (2018). Validation of the unfaulted error bounds for ARAIM. *NAVIGATION*, *65*(1), 117–133. https://doi.org/10.1002/navi.214

Walter, T., Blanch, J., Gunning, K., Joerger, M., & Pervan, B. (2019). Determination of fault probabilities for ARAIM. *IEEE Transactions on Aerospace and Electronic Systems*, *55*(6), 3505–3516. https://doi.org/10.1109/TAES.2019.2909727

Wu, Y., Liu, X., Liu, W., Ren, J., Lou, Y., Dai, X., & Fang, X. (2017). Long-term behavior and statistical characterization of BeiDou signal-in-space errors. *GPS Solutions*, *21*(4), 1907–1922. https://doi.org/10.1007/s10291-017-0663-0

Wang, S., Zhai, Y., & Zhan, X. (2021). Characterizing BDS signal-in-space performance from integrity perspective. *NAVIGATION*, *68*(1), 157–183. https://doi.org/10.1002/navi.409

Xue, B., Wang, H., & Yuan, Y. (2021). Performance of BeiDou-3 signal-in-space ranging errors: accuracy and distribution. *GPS Solutions*, *25*(1). https://doi.org/10.1007/s10291-020-01057-z

Yang, D., Yang, J., & Xu, P. (2017). Timeslot scheduling of inter-satellite links based on a system of a narrow beam with time division. *GPS Solutions*, *21*(3), 999–1011. https://doi.org/10.1007/s10291-016-0587-0

Zhou, S., Hu, X., Liu, L., Guo, R., Zhu, L., Chang, Z., Tang, C., Gong, X., Li, R., & Yu, Y. (2016). Applications of two-way satellite time and frequency transfer in the BeiDou navigation satellite system. *Science China Physics, Mechanics & Astronomy*, *59*(10). https://doi.org/10.1007/s11433-016-0185-6

How to cite this article: Zhang, H., Jiang, Y., & Yang, L. (2023). Preliminary analysis of BDS-3 performance for ARAIM. *NAVIGATION, 70*(1). https://doi.org/10.33012/navi.553